Root Cause Analysis of AC Overcurrent in July 2020 San Fernando Disturbance

Lingling Fan, *Senior Member, IEEE*, Zhixin Miao, *Senior Member, IEEE*

***Abstract*—On July 7 2020, approximately 1,000 MW reduction in solar photovoltaic (PV) output was experienced by the bulk power system in Southern California after a three-phase fault. Disturbance analysis indicates that instantaneous AC current caused inverter tripping. The projection of the root cause of AC overcurrent from the NERC report [1] is that inverter current control is not tight. This letter provides a quantitative analysis on ac overcurrent and addresses the following questions: (i) what type of current controls may lead to ac overcurrent; and (ii) how controller parameters and grid strength may influence ac overcurrent. The letter provides frequency-domain analysis and time-domain simulation results of a grid-integrated inverter to illustrate the effect of control parameters and grid strength on ac overcurrent.**

***Index Terms*—Solar Photovoltaic (PV) grid integration; ac overcurrent; proportional resonant control**

I. Introduction

ON July 7 2020, approximately 1,000 MW reduction in solar photovoltaic (PV) output was experienced by the bulk power system in Southern California after a three-phase fault. Disturbance analysis indicates that instantaneous AC current over 150% of rated value caused inverter tripping. The root cause of ac overcurrent, according to the NERC report [1], is that inverter current control is not tight, which leads to instantaneous ac overcurrent at low ac voltage conditions.

According to [2], two types of current controls are popular: the synchronous dq-frame proportional integral (PI) current control and stationary-frame proportional resonant (PR) current control. In addition, voltage feedforward is often time adopted to decouple the converter from external grid transients [3]. This letter first examines which type of control structure may lead to ac overcurrent in Section II. The speculation of the particular control structure is the stationary-frame PR control without voltage feedforward.

In Section III, the frequency-domain analysis is provided along with time-domain simulation results to examine the effect of PR control parameters and grid strength on ac overcurrent. Section IV concludes the paper.

II. Converter current control structures

A circuit representing a grid-connected voltage-sourced converter (VSC) is presented in Fig. 1. The VSC is connected to the point of common coupling (PCC) bus through a choke filter (its resistance and inductance are notated as R_f and L_f). The grid viewed from the PCC bus is represented by an ideal voltage source, also known as an infinite bus, behind a source impedance $R_g + sL_g$. The VSC's voltage is notated as v and the output current is notated as i.

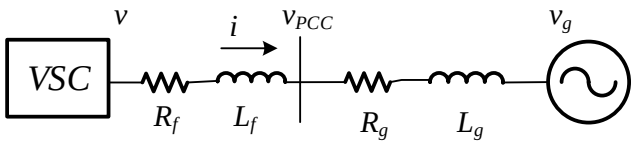

Fig. 1: A grid-connected VSC.

Fig. 2 presents the two types of converter current control structures.

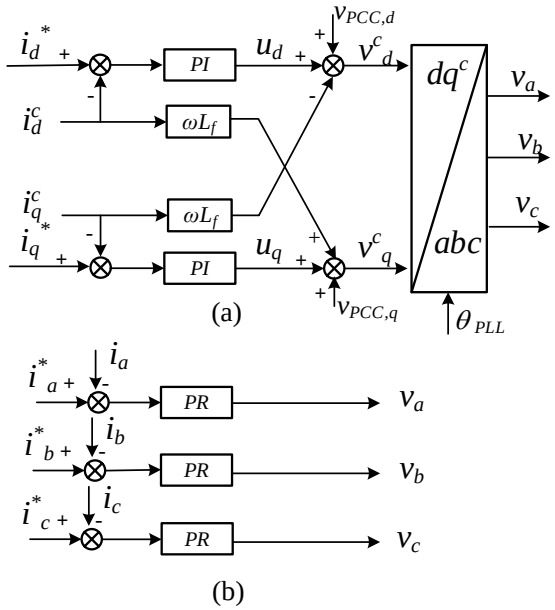

Fig. 2: Dq-frame PI control and stationary-frame PR control.

Fig. 2(a) is the dq-frame based current control. This control structure is similar as Fig. 5 of [2]. The dq-frame is aligned with the PCC voltage's space vector at steady state. The PCC voltage's angle is sensed by a phase-locked-loop (PLL) and the output angle of the PLL is notated as θ_{PLL}. The dq-frame current control consists of PI controllers, the cross-coupling terms, and the PCC voltage feedforward unit. Fig. 2(b) presents the stationary-frame based PR control. This structure is similar as Fig. 7 in [2].

Besides the different frames, there is another significant difference between the two control structures: voltage feedforward. In the dq-frame structure, voltage feedforward is used.

This project is supported in part by US Department of Energy Solar Energy Technology Office DE-EE-0008771. L. Fan and Z. Miao are with the Department of Electrical Engineering, University of South Florida, Tampa, FL, 33620. e-mail: linglingfan@usf.edu.

On the other hand, in the stationary-frame control, voltage feedforward is not used.

The effect of voltage feedforward has been shown in [3] using time-domain simulation. With voltage feedforward, converter current is subject to much less transients even if there are transients in the grid voltage. The authors [3] commented that the converter behaves as a current source with voltage feedforward. This point was confirmed by the authors' research in [4] where the Norton circuit representation of a VSC equipped with the dq-frame current control is derived mathematically. With voltage feedforward considered and with PLL dynamics ignored, the VSC is a current source only.

Remarks: Thus, it is plausible to speculate that voltage feedforward may not exist or may become ineffective in the current control structure of the solar PV inverters of St. Fernando disturbance.

III. Analysis

The PR control in [2] has a transfer function $K_p + \frac{K_r s}{s^2+\omega^2}$ where ω is the nominal frequency. In this study, a more practical PR control is adopted [5]. The transfer function of the PR control is

$$\text{PR}(s) = K_p + K_r \frac{2\omega_c s}{s^2 + 2\omega_c s + \omega^2}. \tag{1}$$

where ω is the nominal frequency 377 rad/s and ω_c is $2\pi \times 2$ rad/s. With the stationary-frame PR control, a converter can be viewed as an impedance: $Z_{\text{VSC}} = \text{PR}(s)$.

The inverter is connected to a grid represented by a voltage source v_g through an impedance $R + Ls$. R includes both the source resistance R_g and the choke filter resistance R_f. L includes both the source inductance L_g and the choke filter inductance L_f. The total impedance viewed from the grid voltage is

$$Z = Z_{\text{VSC}} + Z_{\text{network}}, \tag{2}$$

where $Z_{\text{network}} = R + Ls$.

Based on the PR control structure presented in Fig. 2(b), it is easy to see that $i_a = v_a/(R + Ls)$; thus, the closed-loop transfer function from the current order i_a^* to the current measurement i_a is:

$$\frac{i_a(s)}{i_a^*(s)} = \frac{\text{PR}(s)\frac{1}{R+Ls}}{1 + \text{PR}(s)\frac{1}{R+Ls}} = \frac{Z_{\text{VSC}}}{Z_{\text{network}} + Z_{\text{VSC}}} \tag{3}$$

Fig. 3a presents the impedance of the VSC Z_{VSC}, or the transfer function of PR. It can be seen that the Bode diagram's magnitude has a peak at 60 Hz due to the resonant control which aims for a large gain at 60 Hz at open loop. The current can be expressed by the grid voltage as follows. The subscript a is dropped hereafter for concise expressions.

$$\frac{i(s)}{v_g(s)} = -\underbrace{(Z_{\text{VSC}} + Z_{\text{network}})^{-1}}_{Y} \tag{4}$$

where Y is the total admittance viewed from the grid voltage.

The resulting closed-loop transfer function in (4) is $-Y$. It has the same magnitude as the total admittance Y viewed at the grid. Fig. 3b presents the close-loop system transfer

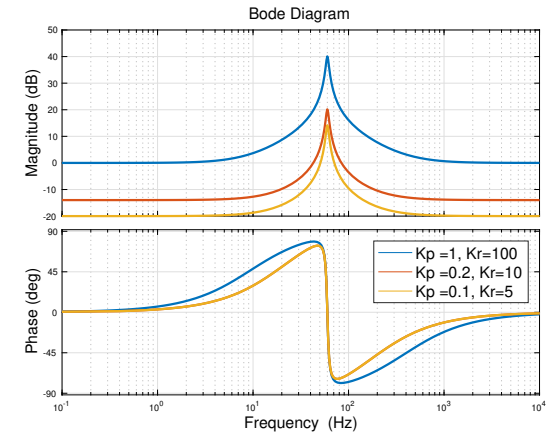

(a)

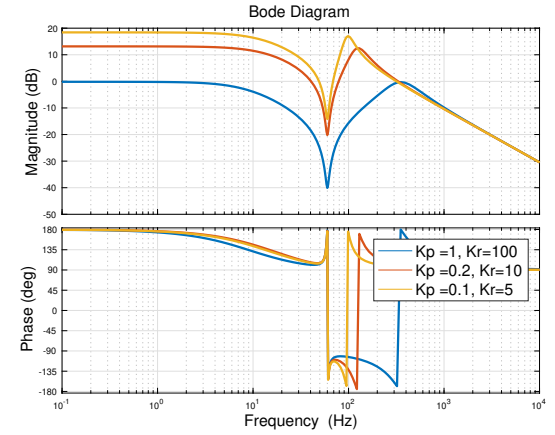

(b)

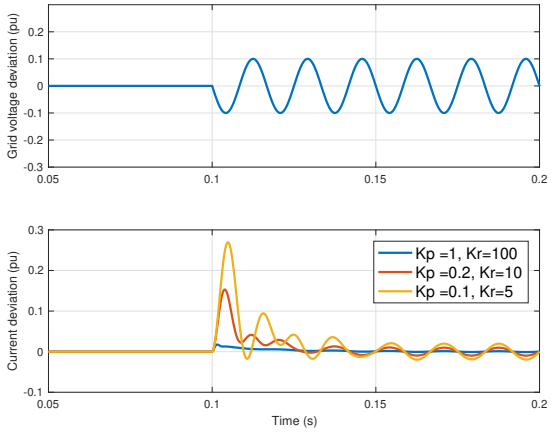

(c)

Fig. 3: (a) Z_{VSC}, or PR control transfer function. (b) The closed-loop system $-Y$. The network impedance is $R + Ls$ where $R = 0.02$ and $L = 0.2/\omega$. (c) Time-domain simulation results. Upper row: grid voltage deviation: 0.1 p.u. dip in magnitude. Lower row: current deviation.

function $-Y$ with the network impedance being $0.02 + j0.2$ pu at the nominal frequency ($L = 0.2/\omega$). At 60 Hz, the Bode diagram's magnitude has a dip, corresponding to the peak in Z_{VSC}.

Remarks: The dip in the closed-loop transfer function $-Y$ means that for a voltage disturbance of 60 Hz, the current will experience a very small change. The smaller the magnitude of $-Y$ at 60 Hz and beyond, the control is more effective in

tracking current order regardless of grid voltage disturbance. Thus, it can be seen that larger PR controller gains mean tighter current control.

Following that dip, a peak shows in the magnitude in the frequency range of 60 Hz—500 Hz. Three sets of control parameters are examined. It can be seen that smaller gains lead to smaller magnitudes in Z_{VSC}; and larger magnitudes of $-Y$ at the peak frequency. The closed-loop system is simulated for a grid voltage dip of 0.1 p.u. of 60 Hz frequency. The current deviation is presented in Fig. 3c. The simulation results show that a smaller gain in PR control indeed leads to a larger ac overcurrent, corresponding to a higher peak in $-Y$'s magnitude plots.

Remarks: Smaller gains of the PR controller, or current control being not tight, will lead to larger overcurrent for the same voltage disturbance.

From the control theory perspective, tight or less tight control refers to order tracking responding time, which can be quantitatively described by bandwidth of the closed-loop transfer function from the order to the measurement (3). The bandwidth of current tracking of a tight control is higher compared to that of a less tight control. In Fig. 4, both frequency responses and time-domain responses of the current tracking closed-loop system in (3) are presented for three sets of PR parameters. It can be seen that the larger gain leads to a higher bandwidth, a faster current order tracking response, or a tight control.

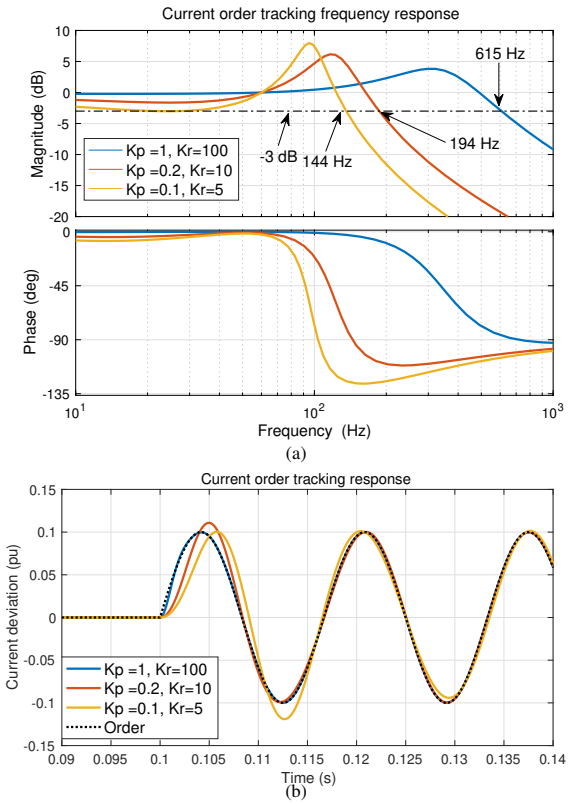

Fig. 4: (a) Frequency responses of (3). (b) Time-domain responses of current order tracking.

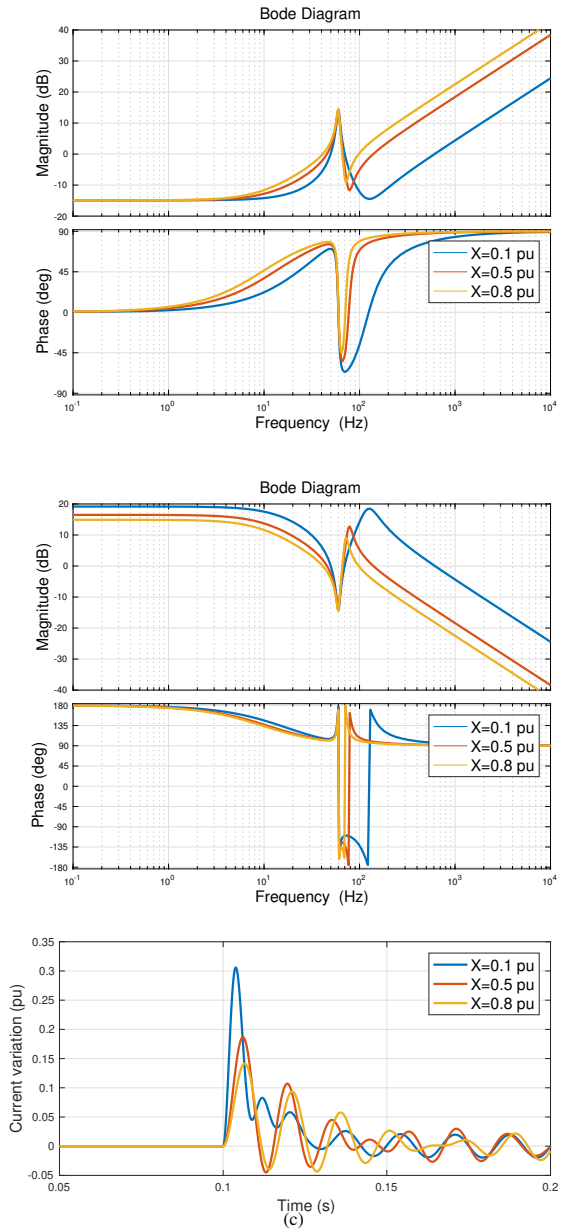

Fig. 5: (a) Bode diagram of the total impedance Z. (b) The closed-loop transfer function $-Y$. (c) Simulation results of the current for 0.1 pu magnitude reduction in the grid voltage.

Further sensitivity analysis is conducted to examine the effect of source impedance on ac overcurrent. The PR control's parameters are fixed at $K_p = 0.1$ and $K_r = 5$ while three source reactance are used: 0.1, 0.5, and 0.8. In each case, $R = 0.1X$. Fig. 5a presents the total impedance Z for the three cases and Fig. 5b presents the closed-loop transfer function $-Y$. The time domain simulation results for a 0.1 p.u. dip in the grid voltage are shown in Fig. 5c. The results confirm that smaller network impedance leads to greater ac overcurrent.

It can be seen that the dip at a frequency point greater than 60 Hz in the impedance magnitude plot in Fig. 5a is due to the interaction of the network impedance $R + Ls$ and the PR control. A small network impedance leads to a small gain at this dip point. In turn, in the closed-loop transfer function $-Y$ plot in Fig. 5b, a smaller network impedance leads to a

larger gain at the peak point greater than 60 Hz. On the other hand, at the 60 Hz point, difference in network impedance has negligible impact on the total impedance Z and the overall $-Y$ since a PR control's gain at the resonant frequency point is very large (see Fig. 3a).

These frequency response characteristics are reflected in the time-domain responses of Fig. 5c. Close to 0.2 s at the steady-state 60 Hz operating condition, the magnitudes of the current for three network impedances become the same. During the initial transient, the small network impedance leads to a high overcurrent, corresponding to a larger peak in $-Y$'s magnitude at a frequency greater than 100 Hz.

IV. Conclusion

This letter provides a quantitative analysis to confirm that ac overcurrent becomes severe if the current control is not tight. The letter also speculates that voltage feedforward may not exist or may be ineffective in those tripped solar PV inverters in St. Fernando disturbance.

References

[1] Joint NERC and WECC Staff Report. (2020, November) San Fernando Disturbance, South California Event: July 7, 2020.

[2] F. Blaabjerg, R. Teodorescu, M. Liserre, and A. V. Timbus, "Overview of control and grid synchronization for distributed power generation systems," *IEEE Transactions on Industrial Electronics*, vol. 53, no. 5, pp. 1398–1409, 2006.

[3] A. Yazdani and R. Iravani, *Voltage-sourced converters in power systems*. Wiley Online Library, 2010, vol. 39.

[4] L. Fan, Z. Miao, and M. Zhang, "Subcycle overvoltage dynamics in solar pvs," *IEEE Transactions on Power Delivery*, pp. 1–1, 2020.

[5] D. N. Zmood and D. G. Holmes, "Stationary frame current regulation of pwm inverters with zero steady-state error," *IEEE Transactions on Power Electronics*, vol. 18, no. 3, pp. 814–822, 2003.